The high flux nano-X-ray diffraction, fluorescence and imaging beamline ID27 for science under extreme conditions on the ESRF Extremely Brilliant Source

Mohamed Mezouar, Gaston Garbarino, Stany Bauchau, Wolfgang Morgenroth, Keith Martel, Sébastien Petitdemange, Pierrick Got, Carole Clavel, Alban Moyne, Hans-Peter van der Kleij, et al.

Taylor & Francis
Taylor & Francis Group

High Pressure Research
An International Journal

ISSN: (Print) (Online) Journal homepage: www.tandfonline.com/journals/ghpr20

The high flux nano-X-ray diffraction, fluorescence and imaging beamline ID27 for science under extreme conditions on the ESRF Extremely Brilliant Source

Mohamed Mezouar, Gaston Garbarino, Stany Bauchau, Wolfgang Morgenroth, Keith Martel, Sébastien Petitdemange, Pierrick Got, Carole Clavel, Alban Moyne, Hans-Peter Van Der Kleij, Anna Pakhomova, Björn Wehinger, Max Gerin, Tomasz Poreba, Lucie Canet, Angelika Rosa, Alexis Forestier, Gunnar Weck, Frédéric Datchi, Max Wilke, Sandro Jahn, Denis Andrault, Lélia Libon, Lea Pennacchioni, Georgii Kovalskii, Markus Herrmann, Dominique Laniel & Hélène Bureau

To cite this article: Mohamed Mezouar, Gaston Garbarino, Stany Bauchau, Wolfgang Morgenroth, Keith Martel, Sébastien Petitdemange, Pierrick Got, Carole Clavel, Alban Moyne, Hans-Peter Van Der Kleij, Anna Pakhomova, Björn Wehinger, Max Gerin, Tomasz Poreba, Lucie Canet, Angelika Rosa, Alexis Forestier, Gunnar Weck, Frédéric Datchi, Max Wilke, Sandro Jahn, Denis Andrault, Lélia Libon, Lea Pennacchioni, Georgii Kovalskii, Markus Herrmann, Dominique Laniel & Hélène Bureau (20 Jun 2024): The high flux nano-X-ray diffraction, fluorescence and imaging beamline ID27 for science under extreme conditions on the ESRF Extremely Brilliant Source, High Pressure Research, DOI: 10.1080/08957959.2024.2363932

To link to this article: https://doi.org/10.1080/08957959.2024.2363932

Published online: 20 Jun 2024.

HIGH PRESSURE RESEARCH
https://doi.org/10.1080/08957959.2024.2363932

Taylor & Francis
Taylor & Francis Group

The high flux nano-X-ray diffraction, fluorescence and imaging beamline ID27 for science under extreme conditions on the ESRF Extremely Brilliant Source

Mohamed Mezouar[a], Gaston Garbarino[a], Stany Bauchau[a], Wolfgang Morgenroth[b], Keith Martel[a], Sébastien Petitdemange[a], Pierrick Got[a], Carole Clavel[a], Alban Moyne[a], Hans-Peter Van Der Kleij[a], Anna Pakhomova[a], Björn Wehinger[a], Max Gerin[a], Tomasz Poreba[a,c], Lucie Canet[a], Angelika Rosa[a], Alexis Forestier[d,e], Gunnar Weck[d,e], Frédéric Datchi[f], Max Wilke[b], Sandro Jahn[g], Denis Andrault[h], Lélia Libon[f], Lea Pennacchioni[b], Georgii Kovalskii[b], Markus Herrmann[g], Dominique Laniel[i] and Hélène Bureau[f]

[a]European Synchrotron Radiation Facility, Grenoble, France; [b]Institut für Geowissenschaften, Universität Potsdam, Potsdam, Germany; [c]Laboratory for Quantum Magnetism, Ecole Polytechnique Federale Lausanne, Lausanne, Switzerland; [d]CEA, DAM, DIF, Arpajon, France; [e]Laboratoire Matière en Conditions Extrêmes, Université Paris-Saclay, CEA, Bruyères-le-Châtel, France; [f]Institut de Minéralogie de Physique des Matériaux et de Cosmochimie (IMPMC), Sorbonne Université, CNRS, UMR 7590, MNHN, Paris, France; [g]Institut für Geologie und Mineralogie, Universität zu Köln, Cologne, Germany; [h]CNRS, IRD, OPGC, LMV, Université Clermont Auvergne, Clermont-Ferrand, France; [i]Centre for Science at Extreme Conditions and School of Physics and Astronomy, University of Edinburgh, Edinburgh, UK

ABSTRACT

In this overview article, we present the main features of the upgraded ID27 beamline which is fully optimised to match the exceptional characteristics of the new Extremely Bright Source (EBS) of the European Synchrotron Radiation Facility (ESRF). The ID27 beamline has been converted to a 120-m-long instrument and has undergone a major refurbishment of all its critical components including both hardware and software environments. We will successively introduce the ID27 undulator X-ray source, optical scheme and the main components of the experimental hutch. We will illustrate the potential of this new instrument through some selected research examples.

ARTICLE HISTORY
Received 30 March 2024
Accepted 31 May 2024

1. Introduction

Static and dynamic high-pressure science is a major research activity at many synchrotrons and free electron laser facilities [1–5]. The high-pressure X-ray diffraction beamline ID27 of the ESRF [6] has been in user mode since 2005 when it replaced ID30 [7], an instrument which was mostly dedicated to white beam experimentation. ID27 stopped operating in 2018 for a full reconstruction in parallel with the implementation of the ESRF Extremely Brilliant Source (EBS) [8]. This instrument was a major resource for the European physics, structural chemistry, materials science and Earth science communities. It was fully

CONTACT Mohamed Mezouar mezouar@esrf.fr European Synchrotron Radiation Facility, 38000, Grenoble, France

optimised for monochromatic high-resolution micro-X-ray diffraction (XRD) to probe materials at very high pressures and temperatures and was exceedingly successful in advancing high-pressure science and technology [9–15]. However, after nearly 12 years of operation, a major upgrade of this instrument was required both to optimally exploit the EBS and to maintain the ESRF position in world-class science. The upgraded high-pressure beamline ID27 is in user operation since November 2021 after 3 years of interruption for its design and construction. This instrument is fully optimised for the EBS and, compared to the former ID27, exhibits much-improved performances in terms of X-ray beam focusing capabilities, intensity, coherence and stability. In addition to the high X-ray beam quality brought by the EBS, the major upgrade of ID27 offers a high-level instrumental environment for users and in-house research experiments. This overview article provides essential information about the key features as well as current and future research activities at ID27.

2. Beamline ID27 – technical configuration

2.1. General beamline configuration

The upgraded high-pressure X-ray diffraction (XRD), fluorescence (XRF) and imaging (XRI) beamline is presented in Figure 1. The pre-existing white beam optics (OH) and experimental hutches (EH1 and EH2) of the former ID27 [6] have been modified and re-used to host all the primary optics of the new instrument. It is composed of three optics hutches OH1 (former OH), OH2 (former EH1) and OH3 (former EH2) located in the experimental hall and a new experimental hutch EH1 housed on the high-quality slab (low-vibration slab) in the 'Chartreuse' hall of the ESRF. The beamline ID27 has been converted to a 110-m-long instrument. This is essential for nano-focusing experiments while keeping

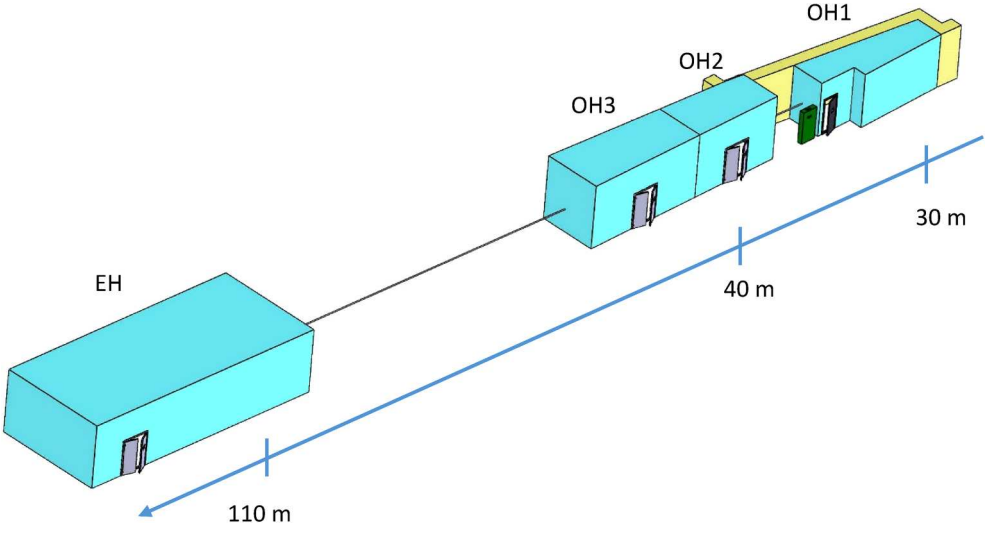

Figure 1. Overall layout of the ID27 beamline. The indicated lengths are the distances between the centre of the straight section of the undulators and the centre of the hutch. OH: Optical Hutch, EH: Experimental Hutch.

Table 1. Beamline configurations.

DMM	DCM	KBM	End-station options
Always in the Beam	No DCM	KB1	Nano-stage for DAC
	Pink beam operation	$15 < E < 25$ keV	Micro-stage for DAC
	$15 < E < 60$ keV	0.3×0.2 μm^2 spot	
		KB2	Nano-stage for DAC
		$E = 33$ keV	Micro-stage for DAC
		0.5×0.35 μm^2 spot	PE and heavy duty
		KB3	Micro-stage for DAC
		$30 < E < 60$ keV	PEP and heavy duty
		2×2 μm^2 spot	
	DCM	KB1	Nano-stage for DAC
	Monochromatic beam operation	$15 < E < 25$ keV	Micro-stage for DAC
	$15 < E < 60$ keV	0.3×0.2 μm^2 spot	
		KB2	Nano-stage for DAC
		$E = 33$ keV	Micro-stage for DAC
		0.5×0.35 μm^2 spot	PEP and heavy duty
		KB3	Micro-stage for DAC
		$30 < E < 60$ keV	PEP and heavy duty
		2×2 μm^2 spot	

Note: DMM: double-multilayer mirrors, DCM: double-crystal monochromator, KBM: Kirkpatrick-Baez mirrors, DAC: diamond anvil cell, PEP: Paris-Edinburgh press.

the maximum space around the pressure cells for the installation of bulky sample environments. Beamline ID27 has a high degree of flexibility, the different beamline configurations are summarised in Table 1.

2.2. ID27 X-ray source

The extremely brilliant source (EBS) provides for the X-ray diffraction beamline ID27 significantly higher photon flux density and higher coherence compared to the former beamline. Now, at photon energies above 30 keV, the energy range most relevant for X-ray diffraction and imaging at extreme conditions, the brilliance and the coherent fraction of the photon flux is increased by almost two orders of magnitude due to the drastic reduction of the horizontal emittance. In addition, large improvements of the shape and width of the undulator harmonics are realised thanks to the upgraded storage ring characteristics. This enables high-flux, medium-resolution ($\Delta E/E \sim 10^{-2}$) XRD and imaging experiments in 'pink' beam mode. The smaller beam divergence in the horizontal direction as shown in Table 2 also largely facilitates the production of high-flux nano-focused beams.

The choice of an optimised insertion device, which fully exploits the outstanding performance of the EBS is fundamental. The primary objective of ID27 is to provide maximum photon flux at X-ray energies between 20 and 35 keV for nano – and micro-XRD. In addition, the source should also perform well at energies down to 15 keV for nano- and micro-fluorescence experiments and at energies up to 60 keV for imaging experiments. An 18-mm period cryo-undulator (CPMU18) [16] placed in the centre of the ID27 straight section was identified as an excellent system in terms of photon flux and tunability. The CPMU18 can operate at a minimum gap of 5 mm (K-value of 2.127). It replaces the two formerly installed U23 in-vacuum undulators. In Figure 2, the performance of a U23 undulator on the EBS is compared to that of a CPMU18 system installed on the EBS. The numerical simulations show a substantial gain in photon flux and a much better tunability in the energy region between 15 and 25 keV.

Table 2. Photon source size and divergence (RMS) from a 2 m-long CPMU18 cryo-undulator installed on the former and current accelerator lattices.

	Direction	source size (μm)	divergence (μrad)
Former ESRF	Horizontal	50	105
	Vertical	6	5
EBS	Horizontal	28	7
	Vertical	4.5	4.5

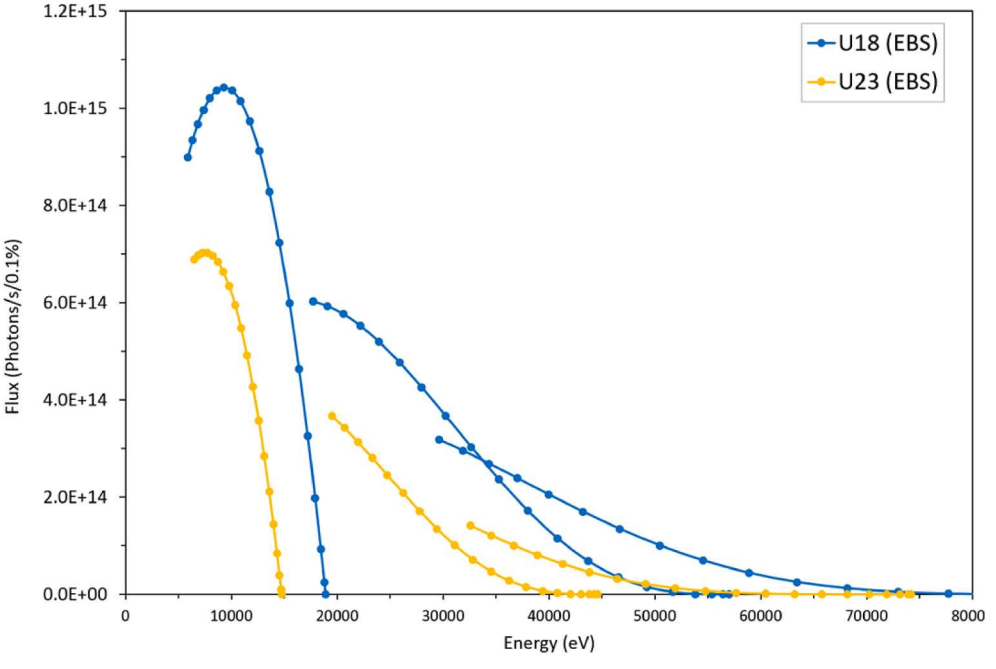

Figure 2. On-axis brilliance for 2-m-long U23 and CPMU18 undulators installed on the EBS. The flux is calculated in a 0.5×0.5 mm^2 slit at 27 m from the X-ray source.

2.3. Optical design

2.3.1. Overall principle

As a basic principle, the number of optical elements is reduced to a minimum in order to improve the stability of the beamline and optimally exploit the intrinsic beam properties. The very low vertical and horizontal emittance of the EBS is a fundamental advantage as compared to the former storage ring. In particular, in the horizontal direction, it enables preserving the brilliance by direct demagnification of the primary source from the CPMU18 without the need of imaging a secondary source. As shown in Figure 3, this leads to a simplified configuration where the first optical element after the primary slits consists of a water-cooled double-multilayer mirror (DMM) in grazing incidence (~4 mrad) and horizontal geometry. The DMM is utilised to produce a 'pink' beam, to partially eliminate the higher harmonics and to reduce the heat load on the downstream optical elements. It is a critical element and particular care must be taken to reduce the deformation (slope errors) induced by the significant heat load from the CPMU18.

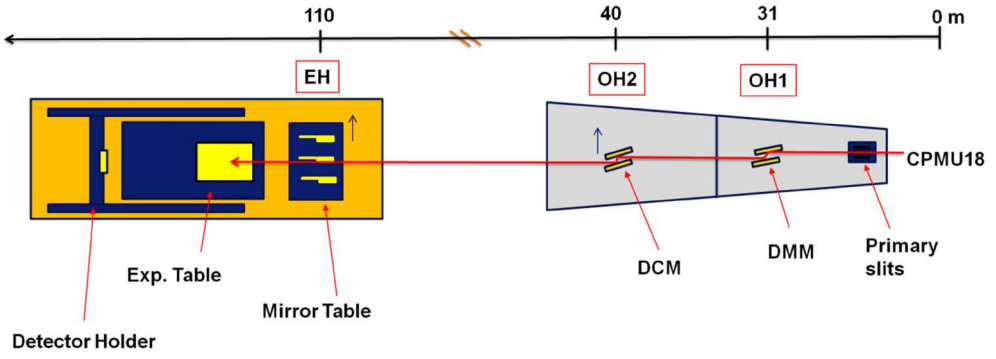

Figure 3. Schematic of the simplified optical configuration of the beamline ID27 (top view). CPMU18: Cryogenic Permanent Magnet Undulator (18 mm magnetic period); DMM: Double-multilayer Mirrors; DCM: Double-Crystal Monochromator. The blue arrow in OH2 indicates the horizontal movement of the DCM that enables 'pink' beam operation.

A Si(111) double-crystal monochromator (DCM) in horizontal geometry with excellent angular stability is used for the high energy-resolution mode. The DCM is liquid nitrogen-cooled to eliminate surface slope errors. Finally, the beam focusing at the sample position is achieved using three Kirkpatrick-Baez (KB) mirror systems [17]. They operate in 'pink' and monochromatic modes to produce X-ray spots of different sizes, different energies and different photon fluxes to fulfil the requirements of the most demanding high-pressure experiments. The targeted high spatial resolution (~250 nm) combined with efficient KB focusing optics and usable working distances result in the choice of a long beamline (120 m).

2.3.2. The double-multilayer mirror (DMM) system hosted in OH1

A water-cooled double-multilayer mirror (DMM) [18] system is employed as 'pink' beam monochromator, to reduce the heat load and radiation level on the downstream optics and for high harmonics rejection. This fixed-exit flat mirrors system is located at 31 m from the undulator X-ray source. The different degrees of freedom of the DMM are indicated in Figure 4. The system supports a variation of the Bragg angle from 0 to 15 mrad, which largely covers the energy domain of interest ($15 < E < 60$ keV). The DMM operates in fixed-exit mode by translating the second mirror along the *x*-axis. The most critical aspect resides in keeping a high short – and long-term angular stability in the vertical and horizontal planes below 150 nrad. As a basic principle, the vibration sensitivity is reduced by composing a very rigid frame made of granite benches within a compact structure. A layout and a photograph of this system are shown in Figure 4. The two mirrors work as narrow energy bandpass filters with $\Delta E/E$ ~2% that enable the reduction of higher harmonics. The mirror reflectivity at the relevant X-ray energies is better than 80%.

Two silicon blocks polished to a flat figure are used as DMM substrates. They include two stripes to cover all required photon energies. In the low energy range from 15 to 25 keV, the simulation shows that a multilayer composed of palladium and graphite is well-suited. At higher energies up to 60 keV, the standard W/B_4C multilayer system is a good choice. Their characteristics and performance are summarised in Tables 3 and 4.

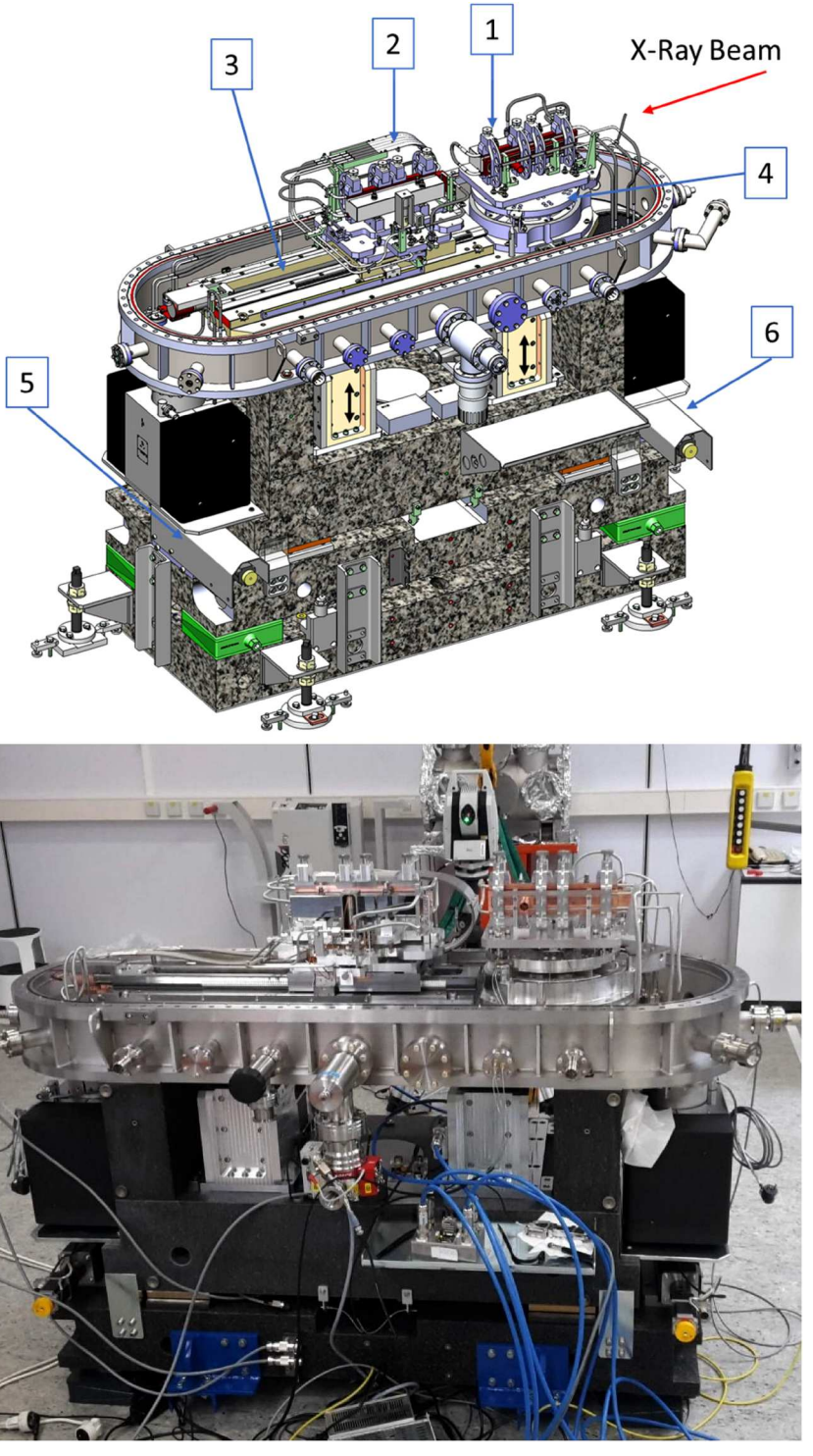

Figure 4. Schematic (top) and photograph (bottom) of ID27 fixed-exit double-multilayer mirror system. 1: First mirror; 2: Second mirror; 3: First mirror mechanics (Pitch); 4: Translation of second mirror along the X-ray beam; 5 and 6: Translations normal to the X-ray beam for Bragg angle and position adjustments. The black arrows indicate the vertical translation hidden inside the granite structure.

Table 3. Characteristics of the low-energy ($15 < E < 25$ keV) DMM stripe.

Material	Thickness [nm]	Density [g/cm^3]	Roughness [nm]
Pd	2.50	10.8	0.35
C (graphite)	4.00	2.6	0.45
E [keV]	θ	R2	$\Delta E/E$
15	0.40° = 6.98 mrad	83%	7.3%
24	0.25° = 4.35 mrad	90%	7.1%

Note: θ: optimal reflectivity angle, R2: Maximum reflectivity, $\Delta E/E$: Energy bandpass.

Table 4. Characteristics of the high-energy ($E > 25$ keV) DMM stripe.

Material	Thickness [nm]	Density [g/cm^3]	Roughness [nm]
W	1.35	16.0	0.30
B_4C	1.70	2.8	0.30
E [keV]	θ	R2	$\Delta E/E$
30	0.40° = 6.98 mrad	72%	2.7%
60	0.20° = 3.49 mrad	86%	2.8%

Note: θ: optimal reflectivity angle, R2: Maximum reflectivity, $\Delta E/E$: Energy bandpass.

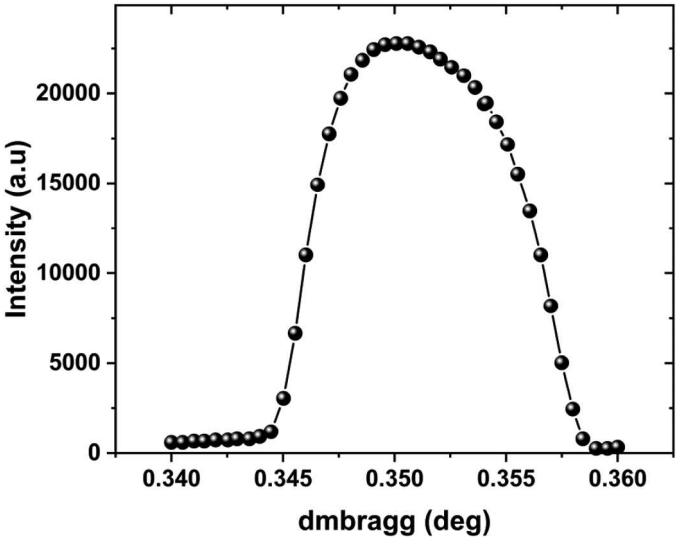

Figure 5. Reflectivity curve of ID27 double-multilayer mirrors.

A reflectivity measurement of the DMM is shown in Figure 5. An energy bandwidth of 2.8% was obtained in excellent agreement with the theoretical prediction.

2.3.3. The double-crystal monochromator (DCM) hosted in OH2

A high-performance fixed-exit liquid nitrogen cooled double-crystal monochromator (DCM) in horizontal geometry from the company AXILON is employed to generate a monochromatic X-ray beam with high energy resolution ($\Delta E/E < 1.5 \times 10^{-4}$) in a wide X-ray energy domain from 15 to 60 keV. This multipurpose DCM is required for high-resolution XRD, X-ray fluorescence and X-ray diffraction imaging experiments. It is located 40 m from the undulator X-ray source and made of two silicon single-crystals with surface

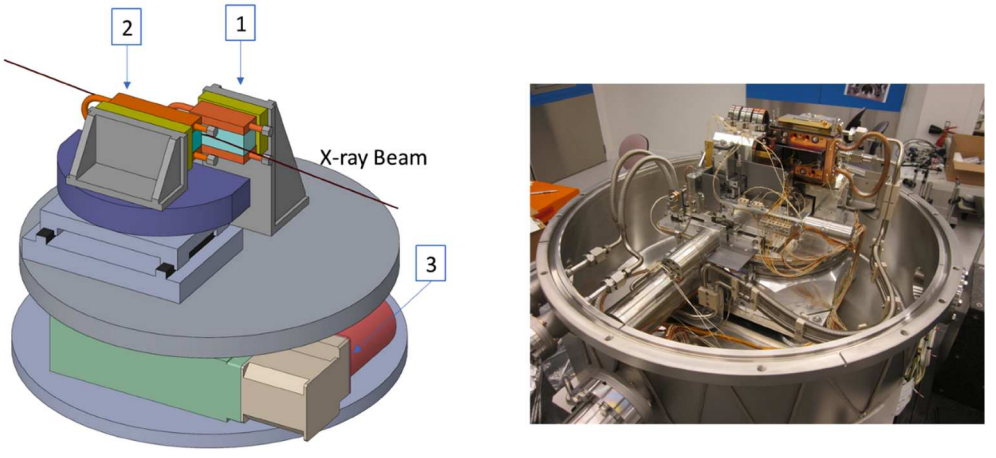

Figure 6. ID27 Si(111) double-crystal monochromator conceptual design (left) and photograph (right). 1: First crystal; 2: Second crystal; 3: Bragg angle mechanics.

roughness lower than 1 Å and oriented along the [111] crystallographic axis. The conceptual design and a photograph of the DCM are shown in Figure 6. It operates in horizontal deflection geometry and requires cutting-edge performance in terms of fixed exit, repeatability, angular, thermal, and long-term stability. The DCM is located after the DMM in the 'pink' beam optics hutch OH2 on a high-stability granite bench. It is possible to easily remove the DCM from the X-ray path using a high-precision horizontal translation to enable 'pink beam' operation.

The different degrees of freedom of the DCM are shown in Figure 6. The system enables a variation of the Bragg angle from 0 to 8 degrees which largely covers the energy domain of interest ($15 < E < 60$ keV) and enables 'pink' beam operation by setting the Bragg angle to 0 degree. The DCM operates in fixed-exit mode by translating the second crystal along the y-axis. As for the DMM, the most critical aspect resides in maintaining a high short- and long-term angular stability in the horizontal plane. This is realized by optimizing the system stiffness and compactness that resulted in an angular stability of the DCM below 150 nrad in both vertical and horizontal directions. The DCM performance is illustrated in Figure 7. The obtained rocking curve at 33.169 keV is very sharp (5.10^{-4} deg. at FWHM), highly symmetric and reproducible, thereby confirming the high stability and quality of the DCM mechanics.

3. End-station – technical overview

3.1. Overall principle

A layout of the experimental end-station is shown in Figure 8. It consists in a multi-modal nano-probe setup designed to accommodate different micro-analytical techniques (XRD, XRF, and XRI) and a variety of sample environments. The new instrument offers much higher spatial resolution (down to ~250 nm) and photon flux compared to the former end-station. It includes three horizontally movable granite tables holding the KB focusing mirrors, three specialised goniometers (heavy duty, nano- and laser-heating goniometers)

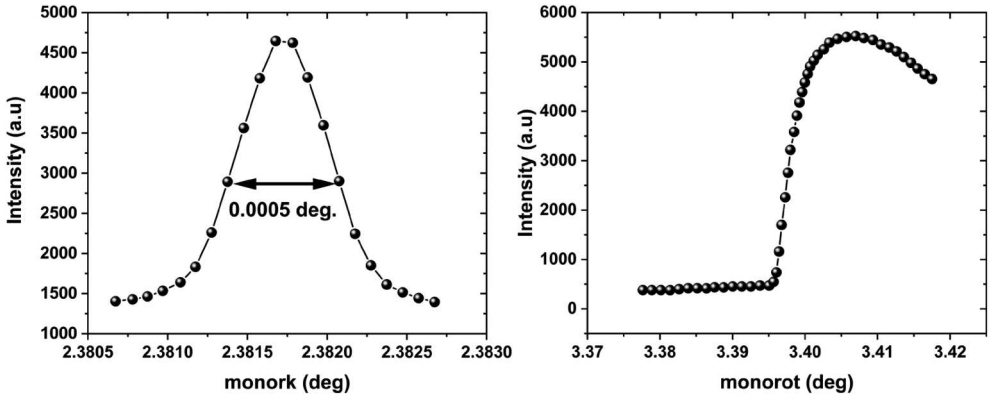

Figure 7. Monochromatic X-ray beam measurements. Left: DCM rocking curve, right: DCM angular scan through the iodine absorption edge at 33.169 keV (K edge).

and a granite holding the detector systems (XRD: Eiger2 9M CdTe from DECTRIS, XRF: Silicon Vortex solid-state detector and XRI: PCO edge camera). In this configuration, the different sample environments do not have to be unmounted when unused. This modularity enables the use of different sample environments during the same experimental run and requests a high degree of positioning precision and reproducibility of the different end-station components. As a basic principle, this is achieved by horizontal encoded translation of pre-aligned devices mounted on highly stable granite tables. This enables an easy and reproducible change of beam operation mode and energy without tedious realignment of the downstream optics and components. The high spatial resolution of the system requires excellent mechanical stability of all the

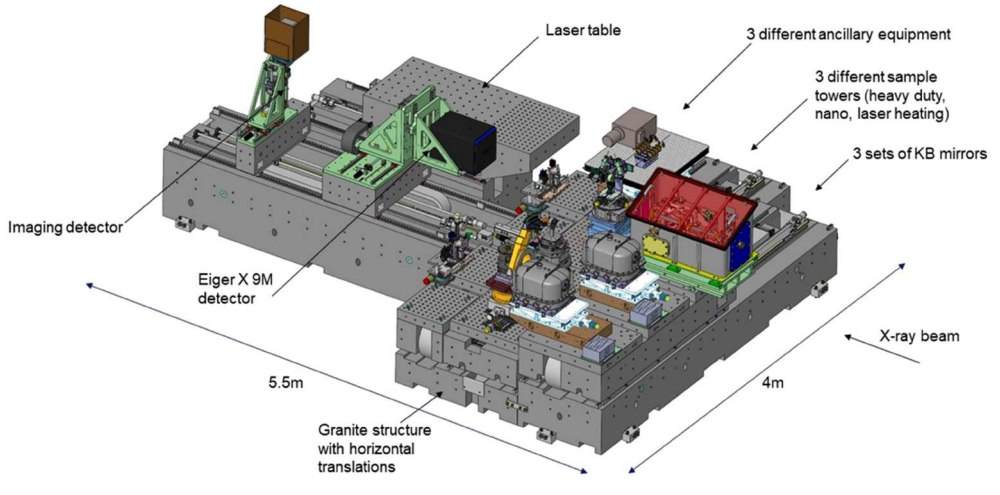

Figure 8. ID27 large (4×5.5 m^2) thermo-stabilized ($\pm$ 0.1 K) experimental setup. Several benches can be operated independently: a mirror granite hosting 3 KB mirror systems for different beam spot sizes and energy domains; a sample granite hosting three goniometers (YAG and CO_2 laser heating, heavy duty (Paris-Edinburgh press, cryostat), and nano-, goniometers); an ancillary equipment granite hosting a pressure by ruby luminescence (PRL) system and a Soller slits system and a detector granite hosting an Eiger2 9M for XRD and a PCO/CMOS for XRI.

mechanical components that hold the sample and the KB-related optics. This level of stability is achieved thanks to high-stiffness stages installed in the thermo-stabilized (± 0.1 K) experimental hutch.

3.2. The Kirkpatrick–Baez (KB) focusing mirrors

A very intense and highly focused high-energy X-ray beam is crucial for *in situ* X-ray diffraction and fluorescence experiments at high pressure because of the very small sample dimensions. For pressures above 200 GPa, typical sample dimensions are of the order of 5 microns. A very small, symmetric, Gaussian-shaped X-ray beam spot of less than 1 micron at full-width half maximum (FWHM) is needed to probe the average properties and a nano-X-ray beam is required for 2D mapping of such demanding samples. This is achieved by using three independent Kirkpatrick–Baez (KB) [18] systems mounted on a single table consisting of a 6 m long, 4.5 m wide and 0.4 m thick granite bed. The table has one degree of freedom (horizontal movement) that adapts the position of the complete instrument to the 'pink' or monochromatic beam mode. The KB mirrors are mounted and aligned reliably with both long-term stability and no inherent vibrational resonances on a common granite base. A long distance (>110 m) between the X-ray source and the focusing mirrors is mandatory for obtaining small beam spots while keeping high flux, high angular resolution (for XRD experiments) and a large working distance to accommodate complex sample environments such as laser-heating systems. The beam spot size at the focal point *f* is the product of the source size *s* times the demagnification *M* and is augmented by the imperfection of the focusing device (*e.g.* slope errors for KB mirrors, imperfect shape for compound refractive lenses). The magnification factor *M* is the ratio of the focal distances *q* and *p*, the distances between the X-ray source and the KB-mirror and between the KB mirrors and the sample, respectively. To fulfil the demand in terms of focal spots and photon flux, three sets of KB-mirrors have been installed at the ID27 end-station for obtaining variable spot sizes from 250 nm to 2 µm (FWHM) in monochromatic and 'pink' beam modes. The main parameters of the KB-systems are summarized in Table 5. They

Table 5. Optical design parameters of the three ID27 KB systems.

	KB1	KB2	KB3
Coating	Pt	W/B_4C	Ir/Al_2O_3
Energy (keV)	15–25	33(fixed)	30–60
Total Transmission	60–70%	74%	64% (at 30 keV)
ΔE/E FWHM	>10%	2%	2%
Length L_h/L_v (mm)	200/200	200/200	300/300
Useful M_h/M_v (mm)	180/180	180/180	250/250
$p_h(m)/q_h(m)$	110/0.35	110/0.60	110/0.8
$p_v(m)/q_v(m)$	110/0.60	110/0.85	110/1.2
Working distance from enclosure (mm)	200	450	600
Incidence angles at centre Maximum	$\theta_h = 2.48$ mrad $\theta_v = 2.71$ mrad $\theta_{max} = 3$ mrad	$\theta_{cen} = 7$ mrad	$\theta = 7$ mrad at 30 keV
Aperture H/V (mm)	0.47/0.5	1.3/1.3	1.8/1.8
Slope errors (nrad)	100	100	300
ideal spot H × V (nm)	200 × 220	400 × 350	1700 × 2000
Spot size from ray tracing H × V (nm)	270 × 220	350 × 500	2000 × 2000

Note: It refers to the ESRF-EBS FWHM source size of $S = 10$ µm (V) × 66 µm (H). The degrading effects of downstream optics are considered. All simulations for KB1 and KB2 assume an average mirror slope error of 100 nrad RMS.

Table 6. X-ray beam size and expected flux at the focal spot of the KB-mirrors in monochromatic and 'pink' beam modes.

Energy (keV)	15 KB1	33 KB2	60 KB3	KB3 at former storage ring
Beam spot size HxV (μm)	0.22×0.28	0.47×0.34	1.2×1.2	2×3
Photons/s $\Delta E/E = 1.5.10^{-4}$ Monochromatic	7.10^{12}	1.10^{13}	$2.2.10^{12}$	$0.9.10^{11}$ (slits 0.2×0.2 mm^2)
Photons/s $\Delta E/E = 2\%$ 'Pink' beam	5.10^{14}	7.10^{14}	1.10^{14}	NA

Note: NA: not applicable.

are obtained assuming a slope error of 0.1 μrad (for KB1 and KB2). The KB1 and KB2 mirrors from the JTEC company have a fixed curvature in order to achieve the highest performance (lowest slope errors). The Pt-coated KB1-system operates in the energy domain from 15 to 25 keV and the multilayer KB2-system provides a fixed energy of 33 keV. The previously existing multilayer KB3 bender system tolerates larger slope errors (>0.3 μrad rms) and generates larger beam spots (1.2×1.2 μm^2) in a wide energy range from 30 to 60 keV.

The photon flux at the focal spot of the KB-mirrors in monochromatic and 'pink' beam modes considering the transmission of all optical elements is listed in Table 6 and compared to that of the former beamline.

3.3. ID27 goniometers

The high spatial resolution of the ID27 instrument requires excellent mechanical stability of the goniometers and granite tables that hold them. A high level of stability is obtained using high-stiffness stages. The KB-mirrors and sample positioners are mounted and aligned on a common granite base to minimize the vibrations of the different components relative to each other. This system has very weak inherent vibrational resonances ensuring excellent long- and short-term stability. The granite tables have only one degree of freedom in the horizontal direction to access the different beamline configurations listed in Table 1. This concept enables an easy and reproducible modification of operation modes and energy without difficult realignment of upstream and downstream devices. Three specialized sample stages are installed on a granite table after the KB-mirrors: a heavy-duty sample stage that hosts either the Paris-Edinburgh cell [7] or the resistively heated diamond anvil setup [19] or the helium-flow cryostat [20], a dedicated stage for laser-heating systems (YAG and CO_2) [21–23] and a nano-positioning stage for 2 dimensional XRD and XRF mapping of micro-samples confined in a diamond anvil cell. They are briefly presented hereafter.

3.3.1. Heavy-duty goniometer

A sketch of ID27 heavy-duty goniometer in the Paris-Edinburgh cell configuration is shown in Figure 9. It is composed of high precision (<1 μm) XYZ and UV translations and a rotation (<10^{-3} degrees). It is designed for a maximum weight of 200 kg and can easily accommodate the Paris-Edinburgh cell, resistively heated diamond anvil cells, or the ESRF-made helium-flow cryostat.

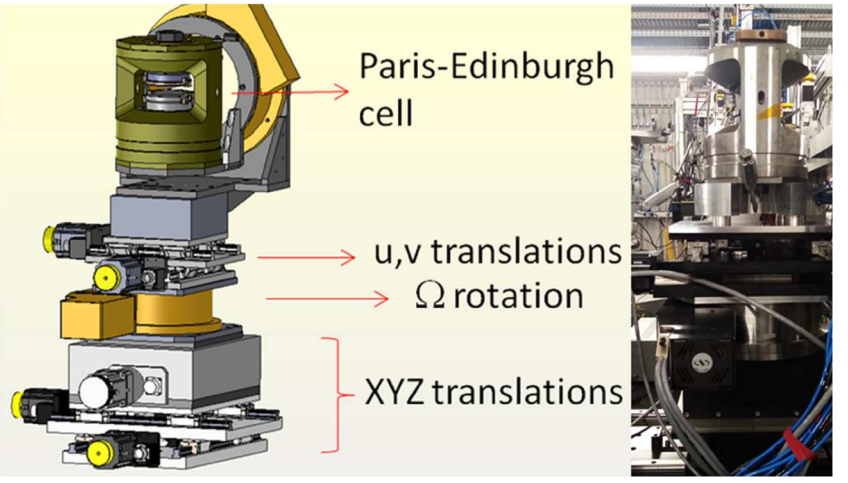

Figure 9. Layout and photograph of ID27 heavy-duty goniometer in Paris-Edinburgh cell configuration.

The goniometer design is largely inspired by the former ID27 system [6]. The main difference is the implementation of linear and circular encoders to enable accurate continuous U, V and Ω scans. The alignment of the sample on the focal point of the KB-systems is realised by a stack of XYZ-motorised translations located below the rotation. The positioning of the sample on the rotation axis of the goniometer is achieved using a second stack (U,V) of translations placed above the rotation.

3.3.2. Laser-heating goniometer

The laser-heated diamond anvil cell (LH-DAC) is the only static technique that can create extreme temperatures (T > 5000 K) at extreme pressure (*P* > 200 GPa). It has been widely used in planetary sciences for the determination of the structure and chemistry of major planetary interior phases [24]. It was also successfully applied to materials science and chemistry [25] for the *in situ* synthesis and characterisation of novel materials and fundamental physics [26], particularly in the study of the liquid state at high pressure – a domain that is still poorly understood. A sketch and a photograph of the laser-heating goniometer are presented in Figure 10. Two YAG laser arms are mounted on a heavy-duty goniometer with characteristics similar to that presented in Section 3.3.1. The positioning of the laser beam is obtained with sub-micron precision by two stacks of XYZ Kohzu motorised translations. In addition to the goniometer, the system is composed of two motorised achromatic Schwarzschild objectives for sample visualisation and temperature measurements, two YAG focal lenses (50, 75 or 100 mm focal distance up- and downstream). More details about the geometry and performance of this setup can be found elsewhere [21].

3.3.1. ID27 nano-positioning goniometer

We have designed and built a nano-positioning goniometer optimised for diamond anvil cells. A layout and a photograph of the system are shown in Figure 11. The nano-positioning system is based on piezo-translations from the Physik Instrumente company and a high-precision LabMotion rotation interfaced to a heavy-duty goniometer which

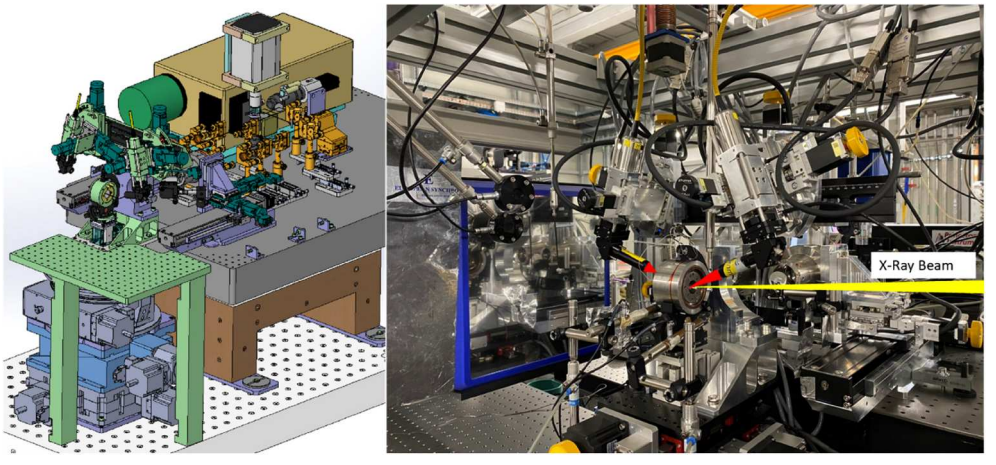

Figure 10. Layout and photograph of ID27 laser-heating system. Red triangles: Laser beams.

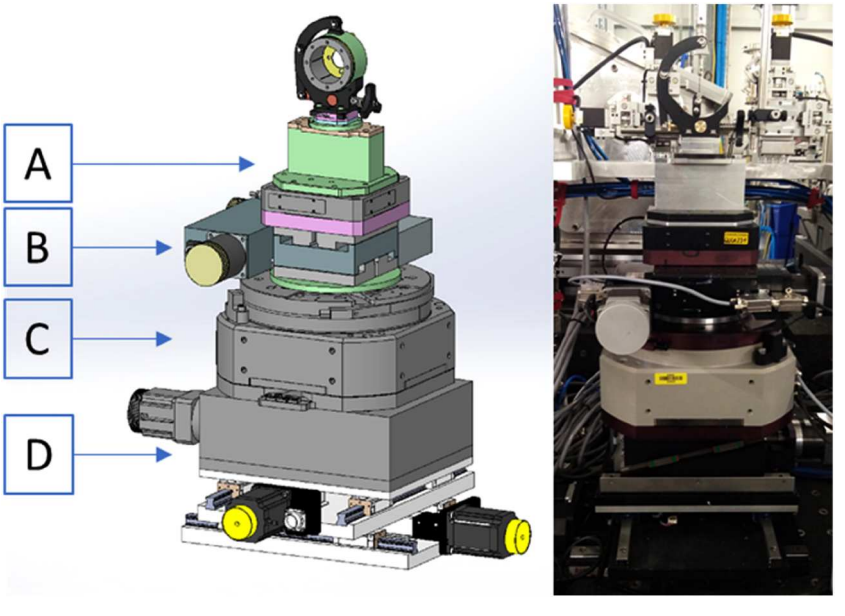

Figure 11. Schematic and photograph of ID27 nano-goniometer for diamond anvil cells. (A) DAC holder and XYZ piezo-stage. (B) XY micro-translation stage. (C) LabMotion aerodynamic rotation. (D) XYZ micro-translation stage.

ensures a sub-micron sample pre-alignment. As it can hold a weight of up to 5 kg, the system is well-suited for 2D nano-XRD and XRF scanning of micro-samples contained in DACs. The main characteristics of the nano-goniometer translations are listed in Table 7.

3.4. Ancillary devices and detector systems

Ancillary devices are essential to perform accurate high-pressure experiments. They are installed on a dedicated versatile horizontally moveable granite table as shown in

Table 7. Specifications of the nano-positioning piezo-system from Physik Instrumente.

Axis	Tx; Ty; Tz
Stroke (µm)	±50
Repeatability (nm)	±20
Resolution (nm)	40

Figure 8. The horizontal movement facilitates easy exchange between different devices. The most important ancillary devices are an on-line pressure by ruby luminescence (PRL) measurement system and a Soller slits setup [27,28]. As already mentioned, three main state-of-the-art detector systems are installed at ID27 to cover all the applications defined in the beamline scientific case. As shown in Figure 12, a high-energy CdTe Eiger2 9M photon counting detector from DECTRIS is permanently installed on a 3-meter-long longitudinally moveable granite table. Additional degrees of freedom are available to translate the system vertically and horizontally. Its main characteristics and performance are listed in Table 8.

As shown in Figure 12, a PCO edge camera for XRI is installed on the same granite bench as the Eiger2 9M detector system and has similar degrees of freedom. The camera is interfaced to an opto-mechanical assembly from the company Optique Peter equipped with magnification optics (up to ×10 for an effective pixel size of ∼1 µm) and a thin fluorescence screen (YAG crystal) to convert the incident X-rays to visible light (Figure 13). The main parameters of the PCO edge (5.5 model) camera are listed in Table 9.

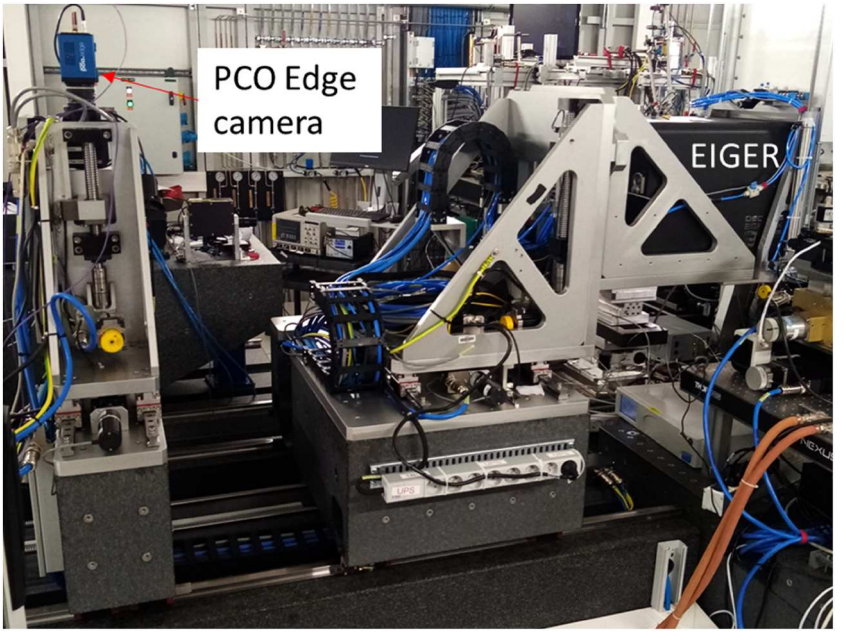

Figure 12. Photograph of ID27 CdTe Eiger2 9M photon counting detector system mounted on high-precision XYZ translation mechanics.

Table 8. Main characteristics and performance of the CdTe Eiger2 9M photon counting detector system.

Parameters	Eiger2 9M system
Number of detector modules	3 × 6
Sensitive area (width × height) [mm^2]	233.2 × 245.2
Pixel size [μm^2]	75 × 75
Total number of pixels	3110 × 3269 = 10166590
Gap width, (H/V) [pixel]	10/37
Inactive area [%]	6.3
Defective pixels [%]	<0.03
Maximum full frame rate [Hz]	238
Counter bit depth [bit]	12
Readout time	Continuous readout, 3 μs dead time
Point-spread function [pixel]	1
CdTe sensor thickness [μm]	450
Threshold energy [keV]	2.7–18
Maximum count rate [phts/s/mm^2]	5.10^8
Image bit depth [bit]	16 or 32
Data format	HDF5 / NeXus
Dimensions (WHD) [mm^3]	340 × 370 × 500
Weight [kg]	41
Power consumption [W]	750

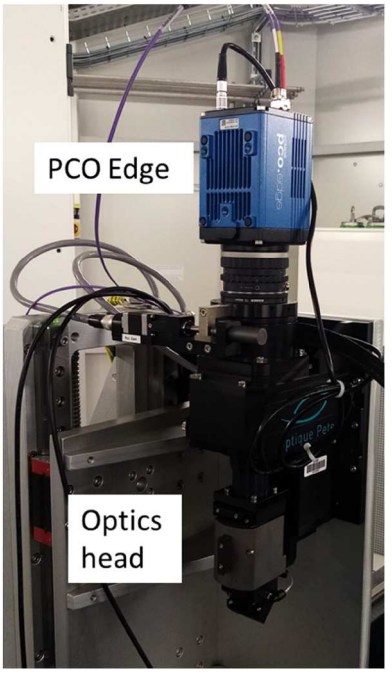

Figure 13. Photograph of ID27 full-field X-ray imaging detector. The PCO Edge 5.5 camera and the optics head for zoom adjustment, X-ray fluorescence screen and mirror.

Silicon Drift Diode (SDD) detectors are robust technologies in terms of count rate capacity and energy resolution. They are routinely used at many synchrotron beamlines in the 5–30 keV energy range. Beamline ID27 is equipped with a 2 mm thick silicon Vortex energy-resolving solid-state detector from the company Hitachi that can be easily installed near the sample goniometers, in forward or backscattering geometry, or close

Table 9. Main characteristics and performance of the PCO Edge 5.5 camera.

Parameters	PCO Edge 5.5
Resolution HxV (pixel)	2560 × 2160
Pixel size HxV (µm)	6.5 × 6.5
Peak quantum efficiency	60%
Dynamic range	12 bits
Readout noise	<0.6 e^-/pixel/s
Maximum full frame rate (Hz)	238
Type of sensor scientific	CMOS (sCMOS)
Data interface	Camera Link

to 90°, for DACs with a large opening in that direction, for the detection of X-ray fluorescence (XRF) signals. As presented in Figure 14, this device is mounted on an XYZ positioning stage for precise alignment and equipped with a silicon polycapillary for confocal detection. The confocal setup is well-suited to diamond anvil cells experiments as it considerably improves the XRF signal-to-noise ratio [29]. This optical device is used as a spatial filter for XRF applications where background radiation originating from areas outside the region of interest interferes with the sample signal. Using the confocal geometry, the spurious radiation background is practically eliminated from the XRF spectrum and, therefore, the detection sensitivity and accuracy are greatly improved.

5. Research examples

5.1. Powder XRD study of superionic ice under extreme P,T *conditions*

In a recent work, the laser-heated DAC setup of ID27 was used to explore the phase diagram of H_2O, a fundamental constituent of giant gaseous planets such as Neptune and Uranus. This type of study is very challenging due to the very small sample size and because water consists of the light elements oxygen and hydrogen that poorly diffract X-rays. As shown in Figure 15, excellent quality X-ray diffraction patterns were obtained at pressures and temperatures in excess of 186 GPa and 2300 K. This represents the highest *P,T* conditions reached by static compression for a detailed structural investigation of H_2O. This experimental achievement was carried out using an optimised boron-doped diamond absorber that enables to create a homogeneous temperature distribution in the whole sample volume probed by the incident X-rays (Figure 15, right). A phase transformation between the well-known bcc ice X and a super-ionic fcc phase

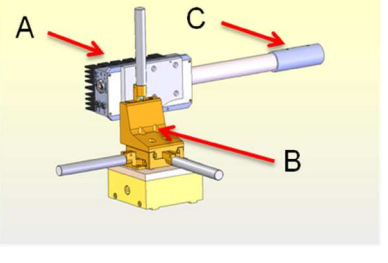

Figure 14. Confocal XRF detecting system. (A) Vortex solid-state detector, (B) XYZ positioning stage, (C) Silicon polycapillary.

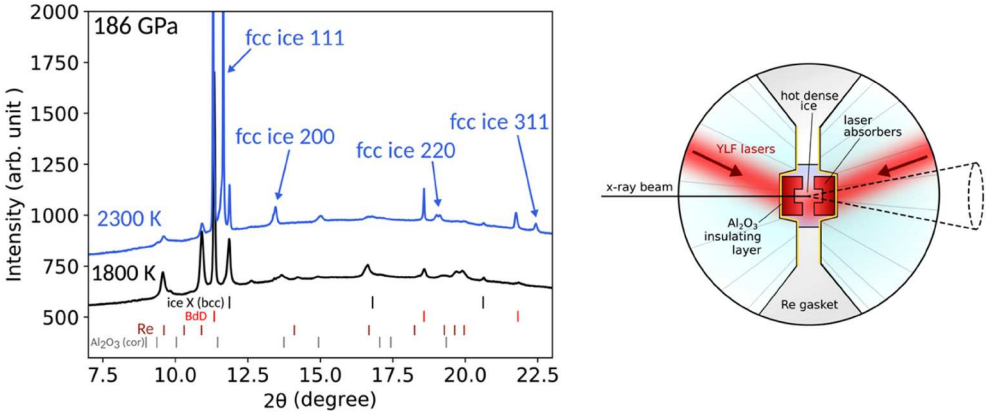

Figure 15. Left: XRD patterns collected at 186 GPa and temperatures of 1800 K and 2300 K, showing the presence of diffraction peaks ('fcc ice') from the super-ionic phase in the diffractogram collected at 2300 K. The tick marks below the diffraction patterns indicate the reflections from the sample assembly. Right: Geometry and details of the assembly contained in the DAC sample chamber including two boron-doped diamond micro-cavities (in red) and a micro-drilled rhenium gasket.

that was previously found at lower *P,T* conditions [30,31] has been observed. The super-ionic form of ice exhibits a rigid oxygen lattice that coexists with mobile hydrogen atoms. This finding is of particular significance as it could explain the intriguing non-dipolar and non-axisymmetric magnetic fields of Uranus and Neptune.

5.2. Synthesis and single-crystal characterisation of novel carbon nitrides

Since the seminal paper of Liu and Cohen [32], the synthesis of novel carbon nitrides has been the focus of intense research. Liu and Cohen predicted that a fully saturated polymeric C_3N_4 solid comprised of corner-sharing CN_4 units could be formed and would have exceptional mechanical properties; likely to have a hardness greater than diamond. In the last three decades, the synthesis of such a material was targeted through a multitude of experimental approaches and yet, only now its formation was reported.

Three novel carbon nitrides, *tI*14-C_3N_4, *hP*126-C_3N_4, and *tI*24-CN_2, all three featuring the necessary building blocks for ultra-incompressibility and superhardness were synthesised in DACs loaded with carbon and nitrogen precursors [33]. These samples were compressed to pressures between 72 and 135 GPa and laser-heated to temperatures above 2000K. In order to determine the structure of these new materials, single-crystal X-ray diffraction (SCXRD) [34] measurements of the resulting micro- and poly-crystals were carried out. The extremely high flux, tightly focussed (*i.e.* 1×1 μm^2) hard X-ray ($\lambda =$ 0.3738 Å, E = 33.169 keV) beam, combined with the EIGER2 X 9M detector available on the ID27 beamline, were essential to obtain the necessary high-quality data to solve the crystal structures of these low-Z materials. In order to pinpoint the location of the highest quality micron- to submicron-sized crystallites of the novel carbon nitrides, an X-ray diffraction map (60×60 steps, with a step size of 0.75 μm) of the complete DAC experimental cavity was first performed. The SCXRD data were then collected in step-scans of 0.5° from −36° to +36° with 5 s per acquisition. The data analysis was performed

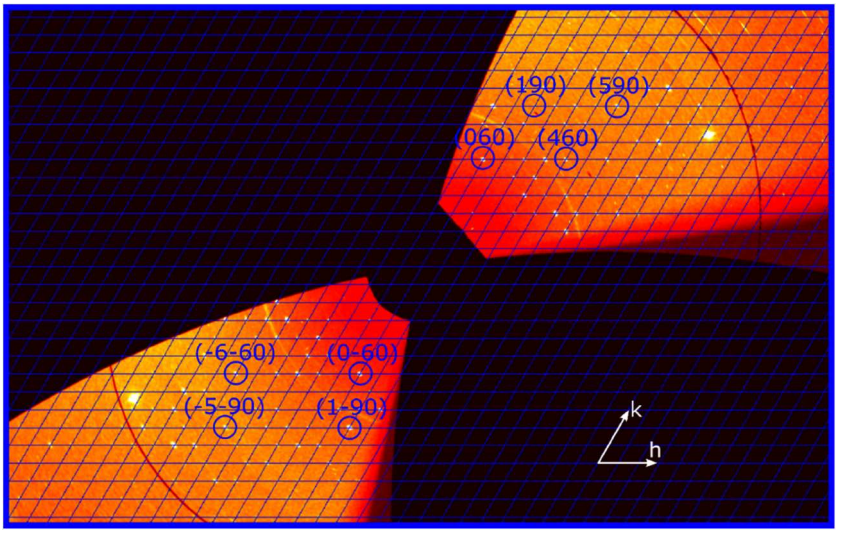

Figure 16. Slice of the (hk0) reciprocal space of a *hP*126-C_3N_4 single crystal at 124 GPa. For clarity, only a few reflections are notated with their corresponding (hkl) index. This figure was taken from reference [33].

onsite employing the Crysalis^{Pro} and OLEX2 software. As seen in Figure 16, sharp and intense diffraction spots were observed and could be indexed to the surprisingly large and complex unit cell of the *hP*126-C_3N_4 compound ($a = b = 17.690(8)$ Å, $c = 2.2645(11)$ Å, alpha = beta = 90°, gamma = 120°; $V = 613.7(5)$ Å^3 at 124 GPa). From these data, a complete structural model was obtained, as shown in Figure 17.

All three C–N compounds were found to be ultra-incompressible, superhard and recoverable to ambient conditions [33]. As such, this research ended a 30-year-long quest for the first fully saturated polymeric C_3N_4 solids featuring CN_4 species and highlights the importance of the upgraded ID27 beamline.

5.3. X-ray fluorescence in the laser-heated DAC

A large fraction of the Earth's core, the outer core, is in the liquid state (Figure 18). In the early ages of the Earth, its mantle was partially molten due to the high energy dissipated by terrestrial accretion. The cooling of this magma ocean led to fractional crystallization into the primitive mantle. Melting conditions and melt compositions of the constituents of the Earth's mantle have been only investigated by *ex situ* petrological and chemical analyses. The combined XRF and XRD setup available at ID27 enables *in situ* chemical analysis of the liquid and solid phases in partially molten systems under extreme *P-T* conditions in the laser-heated DAC. This allows studying the phase relations of the constituents of Earth's mantle and core, providing invaluable information on its present thermal state as well as on the mechanism of early Earth differentiation. Due to the presence of significant thermal gradients in laser-heated micron-sized samples, chemical heterogeneities often occur that are difficult to characterise. Thanks to the intense nanobeams currently available at ID27, this type of 2D analysis can be carried out with a much higher signal-to-noise ratio and spatial resolution.

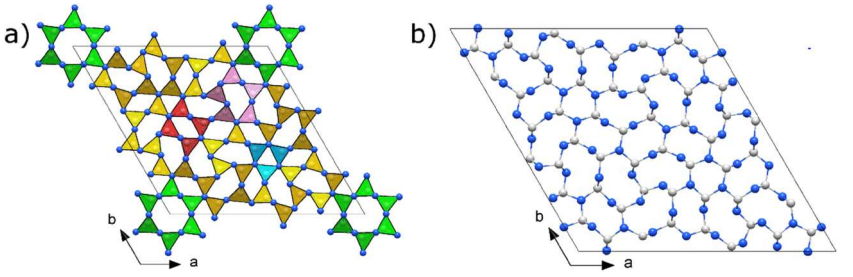

Figure 17. (a) A polyhedral model of *hP*126-C_3N_4 viewed along the *c* direction. The green, pink, red, and teal sets of tetrahedra highlight the six-, five-, four-, and three-membered groups of CN_4 tetrahedra. (b) A projection of the unit cell of *hP*126-C_3N_4 on the *ab* plane. Grey and blue spheres represent carbon and nitrogen atoms, respectively. This figure was taken from reference [33].

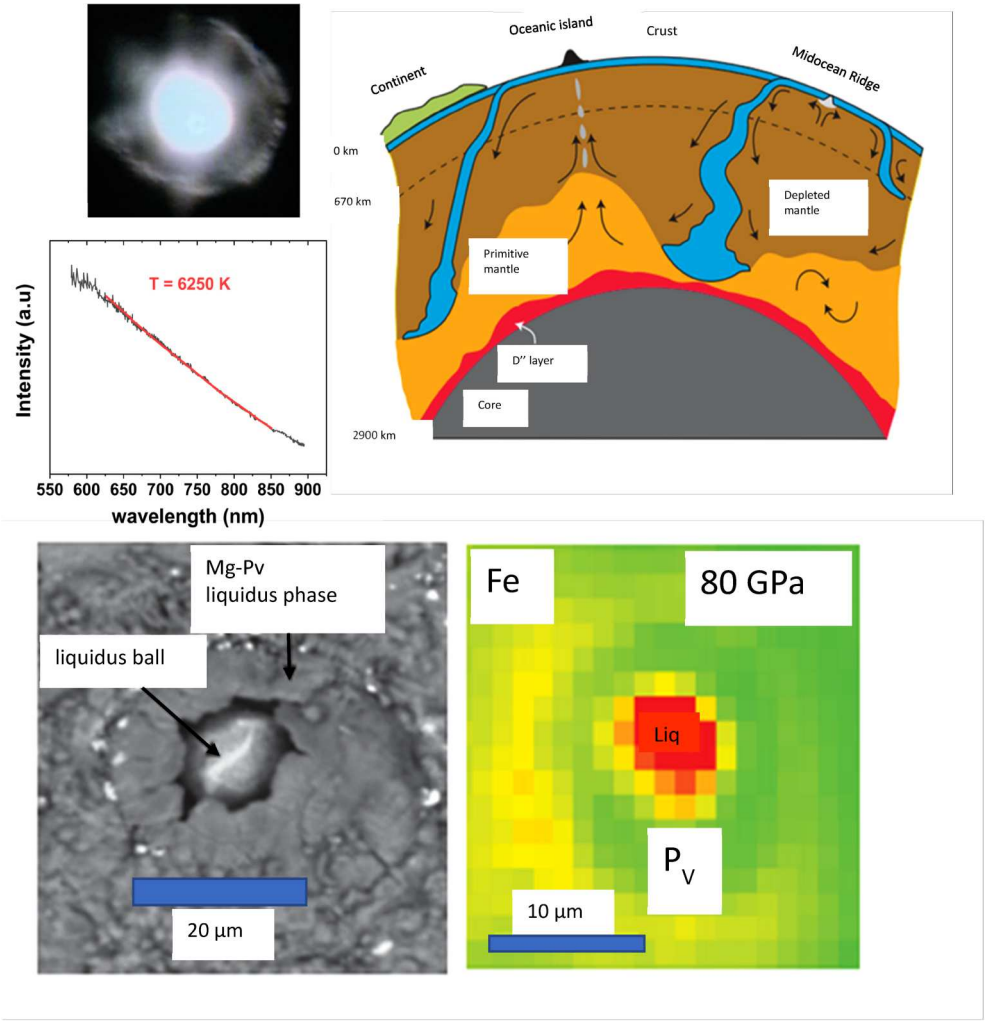

Figure 18. Top: Compressed and laser-heated SiO_2 sample in a diamond anvil cell (left); Schematic of the Earth's interior; Bottom: Heterogeneous laser-heated sample (left), Corresponding ex-situ XRF map (right).

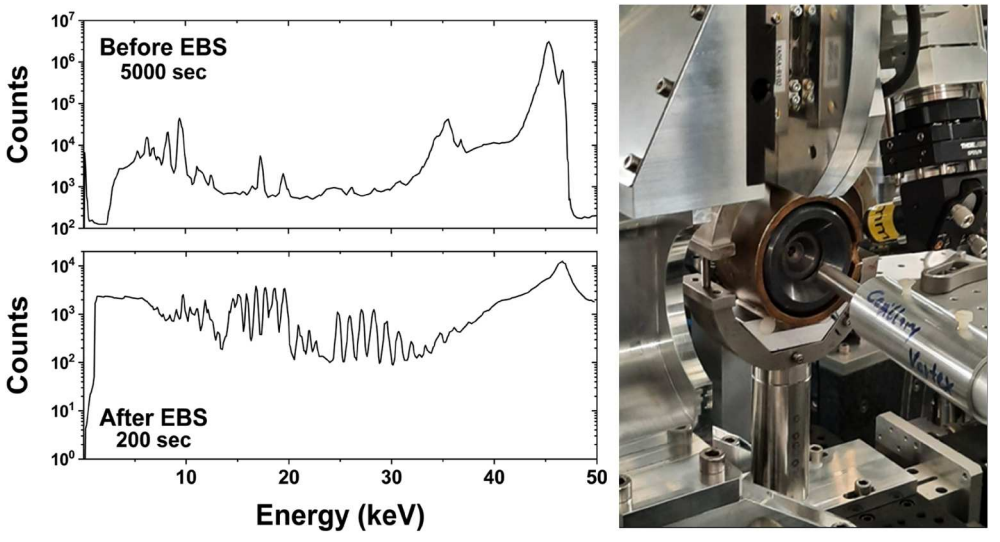

Figure 19. Left: XRF spectra of a glass standard (NIST 610) from the National Institute of Standards and Technology before and after the EBS. This standard contains more than 61 trace elements with concentrations ranging from 50 to 500 ppm. Right: XRF setup interfaced to the laser heating system at ID27.

The new capabilities also have significant applications in extreme conditions chemistry and materials science. Achieving submicron spatial resolution and high dilution levels near or below 1 ppm under extreme *in situ P,T* conditions is currently within reach. This type of study will attain a harvesting stage by combining the exceptional performance of EBS with the new capabilities of the ID27 beamline. The potential of this development is illustrated in Figure 19 in which the improvement in the quality of the XRF signals provided by EBS can be appreciated. These preliminary results were obtained on a standard fluorescence material (NIST610) before and after EBS, respectively. The striking difference in the XRF signal quality is also resulting from the use of a high-sensitivity Vortex solid-state detector interfaced with a confocal polycapillary in backscattering geometry [29]. This device drastically reduces the X-ray background (elastic and inelastic) generated by the sample container and allows the detection of very low concentration levels.

Preliminary tests have been conducted on a strontium and yttrium-doped Fe-bearing haplobasaltic glass sample compressed to 38 GPa and laser heated to temperatures of ca. 1800K. As shown in Figure 20, a significant gain in spatial resolution has been achieved due to the enhanced X-ray beam focusing capability.

These combined XRF-XRD maps cover an area of 80×80 μm^2 using a step size of 1 μm. These maps benefited from the newly available 'standard' small beam size of 0.7 μm at the beamline (using KB2 focusing mirrors). Thanks to the enhanced flux of ID27 and the high sensitivity of the Vortex silicon drift detector, the collection of the individual XRF spectra and XRD patterns in parallel took only 2 s so the complete 2D map was collected within less than 4 hours. The distribution of iron, strontium and yttrium in the sample after laser heating as detected by XRF as well as the XRD intensity at one chosen 2-theta angle are shown in Figure 20. The parallel collection of both signals allows to correlate of the spatial

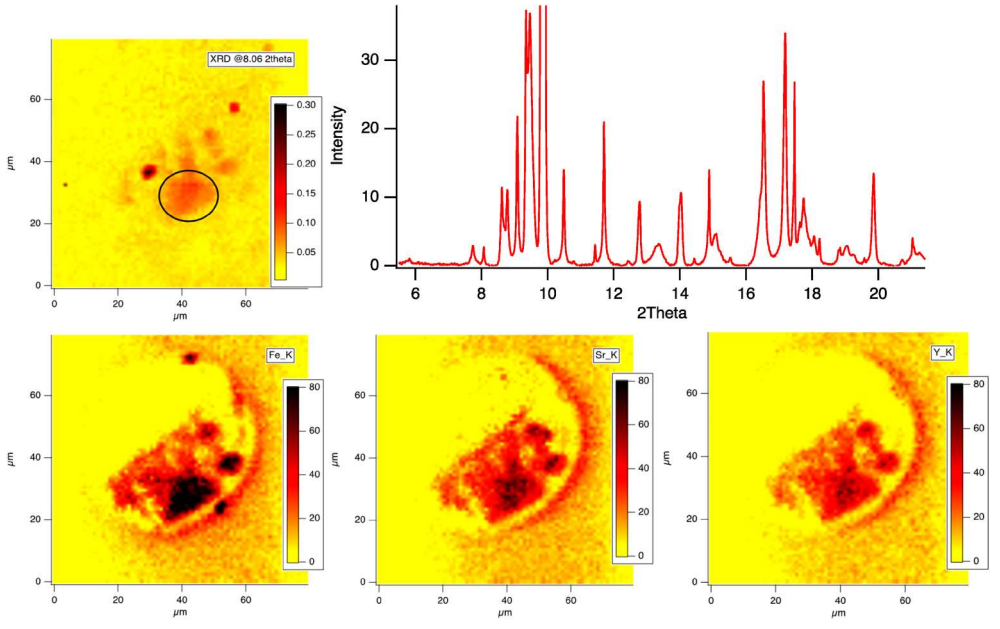

Figure 20. 2D μXRF and μXRD maps measured in parallel on a Fe-bearing bridgmanite glass sample doped with Sr and Y at ca. 5000 ppm level. The data were measured within the DAC after it was laser-heated at several spots at 38 GPa. The XRF detector was set at 75° to the incoming beam and the signal was measured through the side of the upstream anvil. (top left) Intensity map showing the XRD intensity at 8.06° 2theta. The circled area represents a spot that was heated for ca. 15 min. (top right) representative XRD-pattern at a single pixel at the upper rim of the heated area. The pattern can be assigned to bridgmanite and ferropericlase. Bottom: XRF intensity maps of Fe, Sr and Y K-alpha fluorescence. All these elements seem to be enriched in the heated area. The half-circle with enhanced intensity can be assigned to the rim of the Re-gasket, which produces an enhanced background signal, likely due to scattering.

distribution of elements and mineral phases. Particularly, the distribution of trace elements among phases can be visualised *in situ* and without opening the DAC.

5.3. X-ray imaging in the Paris-Edinburgh press

This preliminary experiment aimed at further characterising the low-density (LDL) and high-density liquid (HDL) phases of sulfur in an effort to better understand the driving mechanisms and order parameter of the previously reported liquid–liquid transition (LLT) in the sulfur melt [11]. The main objective here is to determine the shear viscosities η at a few selected *P-T* points in the LDL and HDL. Indeed, a significant and discontinuous increase of η going from LDL to HDL is expected, due to their difference in polymer content. Shear viscosities had been previously measured at ambient pressure [35] and in the range 3.2–9.7 GPa [36], both showing interesting evolutions, but no experimental data existed in the *P-T* range of the LDL nor the HDL close to the LLT line [0.1-2.2 GPa, 450–1050 K]. Viscosity measurements have been obtained using the 'falling sphere' technique [37]. High-purity sulfur powder from Aldrich was packed inside a diamond cylindrical capsule, itself encapsulated into a hBN cylinder capped by two NaCl plates. A platinum sphere of 130–180 μm diameter is deposited on the top centre of the sample below

the NaCl plate. The sphere diameter was determined by optical microscopy and checked using X-ray radiography images. A piece of Pt/hBN mixed powder was also positioned in between the diamond and hBN capsule for *P-T* determination. The sample capsule is then inserted in a graphite cylindrical heater, covered at the two vertical ends with Mo discs. This assembly is put inside a boron–epoxy gasket and two MgO-filled steel rings are placed on the bottom and top end for thermal insulation.

Monochromatic X-rays of 0.3738 Å have been employed. *In situ* radiographic images of the sample were obtained thanks to a PCO Edge fast camera capable of capturing images with a frequency of up to 100 Hz (full frame). Preliminary tests determined that an acquisition sequence of 1000 images of 30 ms was optimal in terms of image quality and read/write deadtime. A times 7 magnification enabled to achieve a resolution of 1 µm as effective pixel size. The high quality of the radiographic images can be appreciated in Figure 21. The significant gain in image quality from previous runs at ID27 is related to the higher coherence of the ESRF-EBS and to the improved quality of the upstream optics (monochromator and double-multilayer mirrors) surfaces.

For all studied samples, we first increased pressure to the desired value and then increased temperature to cross the melting line. During each temperature increment, we collected movies with the PCO Edge camera to observe the movement of the sphere. The sample melting could be visually observed by the propagation of the solid/liquid interface. Several movies of 30 s duration each were collected during the full duration of the Pt sphere fall. An example of time-spaced images collected at 0.25 GPa after melting at 420 K is presented in Figure 22.

The imageJ software was employed to determine the position of the centre of the sphere as a function of time. The travelled distance versus time corresponding to the run in Figure 22 is plotted in Figure 23. It exhibits a sigmoid shape with non-linear regions at the beginning and the end of the curve reflecting the acceleration and deceleration of the sphere as it leaves the top of the sample and approaches the bottom of the capsule, respectively. After the initial acceleration stage, the sphere reaches a terminal velocity that shows as a linear section in the distance-time plot. A fit of the velocity in this time domain gives $V = 1.40(2)$ µm/s. The slow movement of the sphere in this case, combined with the fast-paced image acquisition, enabled to achieve a good precision in the velocity. For the measurement conducted at 0.25 GPa and 420 K gives a viscosity of 77(7) Pa s in good agreement with Terasaki et al. [35]. These experiments proved that the large

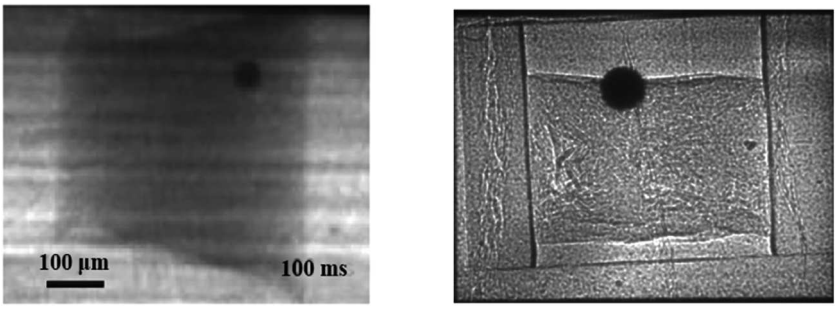

Figure 21. X-ray radiographic images of a platinum sphere in sulfur contained in a diamond capsule before (left) and after (right) the EBS upgrade.

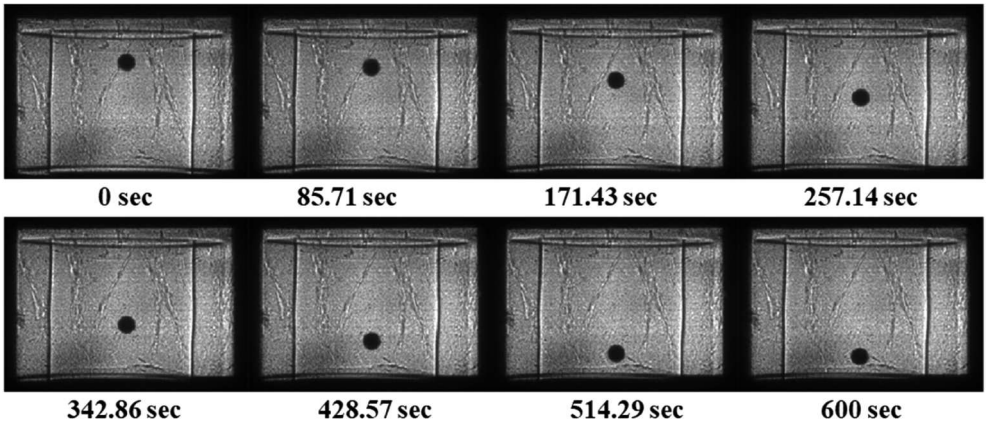

Figure 22. X-ray radiographic images of a sulfur sample during the fall of a Pt sphere at 0.25 GPa and 420 K, as recorded by a PCO Edge camera. The sample/diamond, sample/NaCl and diamond/hBN interfaces can be observed.

improvements in the X-ray imaging capabilities of the new ID27 beamline can be put to profit for viscosity measurements, and will be continued to determine the viscosity variation of liquid sulfur across the liquid–liquid transition.

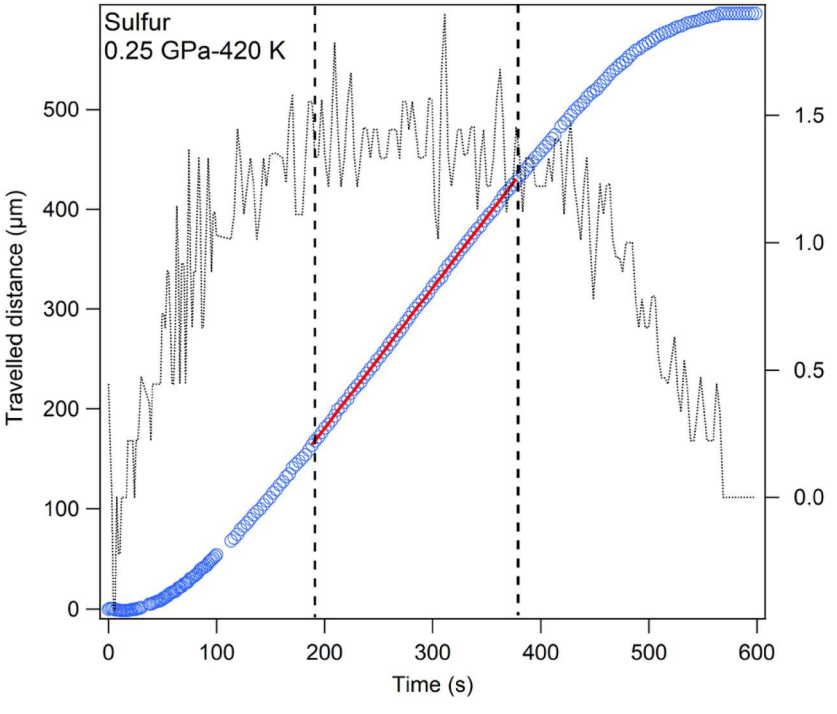

Figure 23. Travelled distance vs. time for the Pt sphere falling in liquid sulfur at 0.25 GPa–420 K and shown in Figure 22. Symbols in blue are experimental data. The black dotted line shows the numerical derivative of the data. The vertical lines delimit the region where the velocity of the sphere is maximal and constant. The red line is a fit of the distance-time plot in this region.

5.4. Structure of glasses and melts using monochromatic and 'Pink' beam mode

Glasses and melts are fascinating systems [38] with unique physico-chemical properties, which have significant fundamental and industrial applications. As for crystalline materials, an accurate structural description is key for understanding their macroscopic properties. The lack of long-range order, the dynamics and the diversity of the chemical composition of glasses and melts constitute important challenges for the unequivocal determination of complete structural models. Progress in this field is often limited by the quality of the X-ray diffraction data which depends on the intensity of the incident X-rays and the maximum achievable Q vector. The 'pink' beam mode that is now available at the ID27 beamline enables to significantly improve these two quantities.

As shown in Figure 24, the strong reduction of the horizontal emittance provided by the EBS resulted in a drastic qualitative improvement of the shape and width of the undulator harmonic. The highly asymmetric harmonics from the former ESRF source have now a highly symmetric pseudo-Voigt profile, which is readily usable for XRD experiments that do not require very high energy resolution. The 'Pink' beam has an energy bandwidth of ~0.5% that is particularly well-suited for glasses and melts studies. In addition, ID27 is equipped with a Soller slits system [27, 28], which acts as a confocal device and enables the collection of X-ray data almost free from contributions of the pressure device itself. This Soller slits system enabled in-house and users research to flourish in new directions, with novel studies of liquids, glasses, or by exploiting the ability to obtain new structure solutions and advanced data refinement techniques on samples under high *P,T* conditions. This device is essential because during high-pressure XRD experiments, the sample is invariably housed within a bulky environment that produces a significant (elastic and inelastic) X-ray background thereby interfering with the XRD signal originating from the sample. This parasitic signal makes XRD experiments on light elements and disordered materials very difficult, if not impossible. An example of its use in monochromatic mode is presented in Figure 25 where high-quality X-ray diffraction patterns of SiO_2 glass measured up to 46.7 GPa are shown.

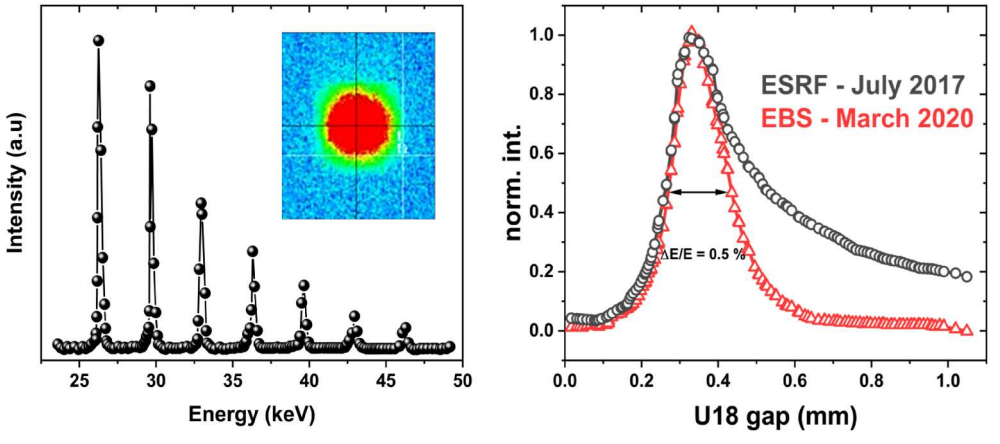

Figure 24. Left: ID27 undulator harmonics after the silicon (111) double-crystal monochromator. Insert image: 'pink' beam observed using an X-ray beam viewer located at 45 m from the EBS X-ray source. Right: Comparison of the shape and width of an undulator harmonic before and after EBS (courtesy of M. Burghammer, ID13, ESRF).

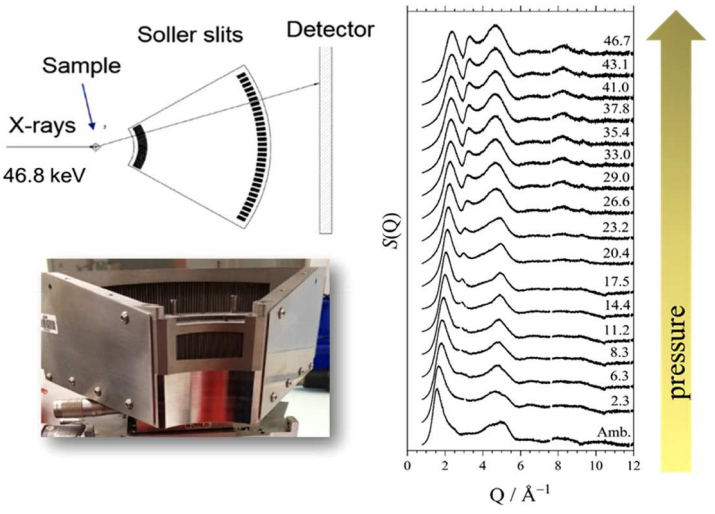

Figure 25. Left: Photograph of ID27 Soller slit system and its basic principle. Pressure evolution of the SiO_2 glass structure factor measured in monochromatic mode up to 46.7 GPa. Exposure time: 90 s.

Thanks to the 2-orders of magnitude gain in intensity, measurements with much higher quality in terms of signal-to-noise ratio can be obtained using the 'pink' beam. A preliminary test comparing monochromatic and 'pink' data is shown in Figure 26. The test sample was liquid argon compressed to 1 GPa in a DAC. The monochromatic and 'pink' beam data were respectively collected in 70 and 1 s, therefore illustrating

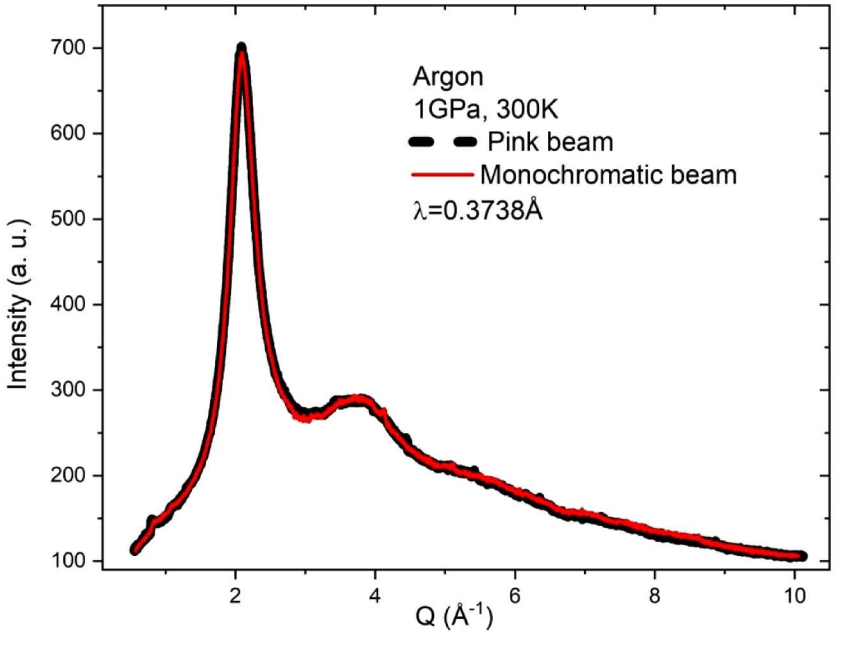

Figure 26. Comparison of monochromatic and 'pink' beam X-ray diffraction of liquid argon contained in a DAC at 1 GPa and room temperature. Exposure time in 'pink' and monochromatic modes were 1 and 70 s, respectively.

the significant gain in intensity. It is also worth noting that no distortion related to the 'pink' mode could be observed reflecting the high symmetry and energy resolution of the undulator harmonics.

Disclosure statement

No potential conflict of interest was reported by the author(s).

Funding

The authors acknowledge the European Synchrotron Radiation Facility for the provision of synchrotron beamtime at the beamline ID27, the support by the Federal Ministry of Education and Research (BMBF) due to an enactment of the German Bundestag under Grants No. 05K2019IP and 05K22IP and by the Agence Nationale de la Recherche (ANR) under grant number ANR-21-CE30-0032-01 (LILI).

References

[1] Sutton SR, Rivers ML, Chariton S, et al. GeoSoilEnviroCARS (Sector 13) at the Advanced Photon Source: a comprehensive synchrotron radiation facility for Earth science research at ambient and extreme conditions. Phys Chem Minerals. 2022;49:32. doi:10.1007/s00269-022-01207-4

[2] Bommannavar A, Chow P, Ferry R, et al. Overview of HPCAT and capabilities for studying minerals and various other materials at high-pressure conditions. Phys Chem Miner. 2022;49:36. doi:10.1007/s00269-022-01209-2

[3] Liermann HP, Konôpková Z, Morgenroth W, et al. The extreme conditions beamline P02.2 and the extreme conditions science infrastructure at PETRA III. J Synchrotron Radiat. 2015;22:908. doi:10.1107/S1600577515005937

[4] Hirao N, Kawaguchi SI, Hirose K et al. New developments in high-pressure X-ray diffraction beamline for diamond anvil cell at SPring-8. Matter Radiat Extremes. 2020; 5: 018403. doi:10.1063/1.5126038

[5] Lotti P, Milani S, Merlini M, et al. Single-crystal diffraction at the high-pressure Indo-Italian beamline Xpress at Elettra, Trieste. J Synchrotron Radiat. 2020;27:222–229. doi:10.1107/S1600577519015170

[6] Mezouar M, Crichton WA, Bauchau S, et al. Development of a new state-of-the-art beamline optimized for monochromatic single-crystal and powder X-ray diffraction under extreme conditions at the ESRF. J Synchrotron Radiat. 2005;12:659–664. doi:10.1107/S0909049505023216

[7] Mezouar M, Le Bihan T, Libotte H, et al. Paris-Edinburgh large-volume cell coupled with a fast imaging-plate system for structural investigation at high pressure and high temperature. J Synchrotron Radiat. 1999;6:1115–1119. doi:10.1107/S0909049599010651

[8] Raimondi P, Benabderrahmane C, Berkvens P, et al. The Extremely Brilliant Source storage ring of the European Synchrotron Radiation Facility. Comm Phys. 2023;6:82-1–82-11. doi:10.1038/s42005-023-01195-z

[9] Anzellini S, Dewaele A, Mezouar M, et al. Melting of iron at Earth's inner core boundary based on fast X-ray diffraction. Science. 2013;340:464–466. doi:10.1126/science.1233514

[10] Andrault D, Petitgirard S, Lo Nigro G, et al. Solid-liquid iron partitioning in Earth's deep mantle. Nature. 2012;487:354–357. doi:10.1038/nature11294

[11] Henry L, Mezouar M, Garbarino G, et al. Liquid-liquid transition and critical point in sulfur. Nature. 2020;584:382–386. doi:10.1038/s41586-020-2593-1

[12] Pépin CM, Geneste G, Dewaele A, et al. Synthesis of FeH5: A layered structure with atomic hydrogen slabs. Science. 2017;357:382–385. doi:10.1126/science.aan0961

[13] Loa I, Nelmes RJ, Lundegaard LF, et al. Extraordinarily complex crystal structure with mesoscopic patterning in barium at high pressure. Nature Mat. 2012;11:627–632. doi:10.1038/nmat3342
[14] Dewaele A, Worth N, Pickard CJ, et al. Synthesis and stability of xenon oxides Xe_2O_5 and Xe_3O_2 under pressure. Nature Chem. 2016;8:784–790. doi:10.1038/nchem.2528
[15] Scelta D, Baldassarre A, Serrano-Ruiz M, et al. Interlayer bond formation in black phosphorus at high pressure. Angew Chem Int Ed. 2017;56:14135–14140. doi:10.1002/anie.201708368
[16] Chavanne J, Lebec G, Penel C. Cryogenic permanent magnet undulators. AIP Conf Proc. 2010;1234:25–28. doi:10.1063/1.3463185
[17] Kirkpatrick P, Baez AV. Formation of optical images by x-rays. J Opt Soc Am. 1948;38(9):766–774. doi:10.1364/JOSA.38.000766
[18] Bigault T, Ziegler E, Morawe C, et al. Double multilayer monochromator to tailor bending magnet radiation spectrum. Crystals, multilayers, and other synchrotron optics. SPIE Proc 5195: 12, 2003; San Diego, USA. doi:10.1117/12.515980
[19] Ritschel T, Stahl Q, Kusch M, et al. Stabilization mechanism of molecular orbital crystals in IrTe2. Comm Phys. 2022;5:325. doi:10.1038/s42005-022-01094-9
[20] Rosa AD, Hilairet N, Ghosh S, et al. *In situ* monitoring of phase transformation microstructures at Earth's mantle pressure and temperature using multi-grain XRD. J Appl Cryst. 2015;48:1346–1354. doi:10.1107/S1600576715012765
[21] Schultz E, Mezouar M, Crichton W, et al. Double-sided laser heating system for in situ high pressure – high temperature monochromatic X-ray diffraction at the ESRF. High Press Res. 2005;25:71–83. doi:10.1080/08957950500076031
[22] Mezouar M, Giampaoli R, Garbarino G, et al. Methodology for in situ synchrotron X-ray studies in the laser-heated diamond anvil cell. High Press Res. 2017;37:170–180. doi:10.1080/08957959.2017.1306626
[23] Giampaoli R, Kantor I, Mezouar M, et al. Measurement of temperature in the laser heated diamond anvil cell: Comparison between reflective and refractive optics. High Press Res. 2018;38:250–269. doi:10.1080/08957959.2018.1480017
[24] Morard G, Boccato S, Rosa A, et al. Solving controversies on the iron phase diagram under high pressure. Geophys Res Lett. 2018;45:11074–11082. doi:10.1029/2018GL079950
[25] Aslandukov A, Jurzick PL, Bykov M, et al. Stabilization of the CN35- anion in recoverable high-pressure $Ln_3O_2(CN_3)$ (Ln = La, Eu, Gd, Tb, Ho, Yb) oxoguanidinates. Angew Chem Int Ed. 2023;62; doi:10.1002/anie.202311516
[26] Dewaele A, Amadon B, Bosak A, et al. Synthesis of single crystals of ε-iron and direct measurements of its elastic constants. Phys Rev Lett. 2023;131; doi:10.1103/PhysRevLett.131.034101
[27] Mezouar M, Faure P, Crichton W, et al. Multichannel collimator for structural investigation of liquids and amorphous materials at high pressures and temperatures. Rev Scient Instr. 2002;73:3570–3574. doi:10.1063/1.1505104
[28] Weck G, Garbarino G, Ninet S, et al. Use of a multichannel collimator for structural investigation of low-Z dense liquids in a diamond anvil cell: validation on fluid H2 up to 5 GPa. Rev Scient Instr. 2013;84; doi:10.1063/1.4807753
[29] Wilke M, Appel K, Vincze L, et al. A confocal set-up for micro-XRF and XAFS experiments using diamond-anvil cells. J Synchrotron Radiat. 2010 Sep;17(5):669–675. doi:10.1107/S0909049510023654
[30] Weck G, Queyroux JA, Ninet S, et al. Evidence and stability field of fcc superionic water ice using static compression. Phys Rev Lett. 2022;128:165701-1–165701-6. doi:10.1103/PhysRevLett.128.165701
[31] Prakapenka VB, Holtgrewe N, Lobanov SS, et al. Structure and properties of two superionic ice phases. Nature Phys. 2021;17:1233–1238. doi:10.1038/s41567-021-01351-8
[32] Liu AY, Cohen ML. Science. 1989; 245: 841-842. doi:10.1126/science.245.4920.841
[33] Laniel D, Trybel F, Aslandukov A, et al. Synthesis of ultra-incompressible and recoverable carbon nitrides featuring CN_4 tetrahedra. Adv Mat. 2024;36:2308030-1–2308030-12. doi:10.1002/adma.202308030

[34] Girard E, Prangé T, Dhaussy AC, et al. Adaptation of the base-paired double-helix molecular architecture to extreme pressure. Nucl Acids Res. 2007;35:4800–4808. doi:10.1093/nar/gkm511
[35] Bacon RP and Fanelli RJ. The viscosity of Sulfur[1]. J Am Chem Soc. 1943; 65: 639. doi:10.1021/ja01244a043
[36] Terasaki H, Kato T, Funakoshi K, et al. Viscosity of liquid sulfur under high pressure. J Phys: Condens Matter. 2004;16:1707. doi:10.1088/0953-8984/16/10/003
[37] Perillat JP, Mezouar M, Garbarino G et al. *In situ* viscometry of high-pressure melts in the Paris–Edinburgh cell: application to liquid FeS. High Press Res. 2010; 30: 415. doi:10.1080/08957959.2010.494844
[38] Berthier L, Ediger MD. Facets of glass physics. Phys Today. 2016;69(1):40. doi:10.1063/PT.3.3052